

Photon Statistics of Propagating Thermal Microwaves

J. Goetz,^{1,2,*} S. Pogorzalek,^{1,2} F. Deppe,^{1,2} K. G. Fedorov,^{1,2} P. Eder,^{1,2,3}
M. Fischer,^{1,2,3} F. Wulschner,^{1,2} E. Xie,^{1,2,3} A. Marx,¹ and R. Gross^{1,2,3,†}

¹Walther-Meißner-Institut, Bayerische Akademie der Wissenschaften, 85748 Garching, Germany

²Physik-Department, Technische Universität München, 85748 Garching, Germany

³Nanosystems Initiative Munich (NIM), Schellingstraße 4, 80799 München, Germany

(Dated: prel. version September 27, 2016)

In experiments with superconducting quantum circuits, characterizing the photon statistics of propagating microwave fields is a fundamental task. We quantify the $n^2 + n$ photon number variance of thermal microwave photons emitted from a black-body radiator for mean photon numbers $0.05 \lesssim n \lesssim 1.5$. We probe the fields using either correlation measurements or a transmon qubit coupled to a microwave resonator. Our experiments provide a precise quantitative characterization of weak microwave states and information on the noise emitted by a Josephson parametric amplifier.

PACS numbers: 42.50.Pq, 02.50.-r, 85.25.Hv

As propagating electromagnetic fields in general [1–3], propagating microwaves with photon numbers on the order of unity are essential for quantum computation [4, 5], communication [6], and illumination [7–10] protocols. Because of their omnipresence in experimental setups, the investigation of propagating thermal states is a fundamental task. Specifically in the microwave regime, sophisticated experimental techniques for their generation, manipulation, and detection have been developed in recent years. In this context, an important aspect is the generation of propagating thermal microwaves using thermal emitters [11–13]. These emitters can be spatially separated from the setup components used for manipulation and detection [14, 15], which allows one to individually control the emitter and the setup temperature. Due to the low energy of microwave photons, the detection of these fields typically requires the use of near-quantum-limited amplifiers [16–18], cross-correlation detectors [13, 14, 19], or superconducting qubits [20–22].

The unique nature of propagating fields is reflected in their photon statistics, which is described by a probability distribution either in terms of the number states or in terms of moments. The former were studied by coupling the field to an atom or qubit and measuring the coherent dynamics [23–25] or by spectroscopic analysis [26]. The moment-based approach, in practice, requires knowledge on the average photon number n and its variance $\text{Var}(n)$ to distinguish many states of interest. To this end, the second-order correlation function $g^{(2)}(\tau)$ has been measured to analyze the photon statistics of thermal [27–29] or quantum [30–32] emitters ever since the ground-breaking experiments of Hanbury Brown and Twiss [33, 34]. While these experiments use the time delay τ as control parameter, at microwave frequencies the photon number n can be controlled conveniently [11, 26, 35–37]. In the specific case of a thermal field at frequency ω , the Bose-Einstein distribution yields $n(T) = [\exp(\hbar\omega/k_B T) - 1]^{-1}$ and $\text{Var}(n) = n^2 + n$, which can be controlled by the temperature T of the emitter. In

practice, one wants to distinguish this relation from both the classical limit $\text{Var}(n) = n^2$ and the Poissonian behavior $\text{Var}(n) = n$ characteristic for coherent states [35] or shot noise [20, 38]. Hence, as shown in Fig. 1, the most relevant regime for experiments is $0.05 \lesssim n \lesssim 1$, which translates into temperatures between 100 mK and 1 K at approximately 6 GHz for the thermal emitter [22].

In this Letter, we experimentally confirm the theoretically expected photon number variance $\text{Var}(n)$ of thermal microwave fields for $0.05 \lesssim n \lesssim 1.5$ using two fundamentally distinct experimental setups. On the one hand, we use a superconducting transmon qubit [39] interacting with the propagating fields via a dispersively coupled microwave resonator. Differently to approaches relying on the coherent dynamics [23–25], in our experiments the change of the qubit dephasing rate induced by the field directly reflects the photon number variance. We furthermore can distinguish between the Poissonian statistics of coherent states and shot noise because the resonator has a different decay constant for these two input fields. On the other hand, we extract the super-Poissonian photon statistics of propagating thermal microwaves from direct correlation measurements and from measurements using a near-quantum-limited Josephson parametric am-

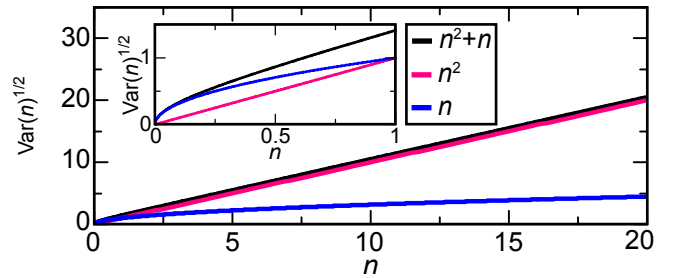


Figure 1. Photon number correlations. $[\text{Var}(n)]^{1/2}$ plotted versus photon number for thermal fields (black), their classical limit (red), and coherent states (blue). The inset shows the regime that we capture in our experiments.

plifier (JPA) [17, 40] as preamplifier. The results show that the noise added by the JPA inevitably alters the photon statistics of the amplified field. Our results provide a quantitative picture of propagating thermal microwaves, which is especially relevant for the characterization of more advanced quantum states in the presence of unavoidable thermal background fields. With respect to superconducting qubits, we gain systematic insight into a dephasing mechanism which may become relevant for state-of-the-art devices with long coherence times [41, 42].

In our experiments, we generate the thermal fields using a temperature-controllable, 50 Ω -matched attenuator acting as a black-body emitter. This emitter is thermally only weakly coupled to the 35 mK base temperature stage of a dilution refrigerator. Heating the attenuator up to 1.5 K results in the emission of thermal microwave radiation, which we guide to our detection setups. Experimentally, we achieve a high photon number stability $\delta n/n \lesssim 0.01$ due to the precise temperature stabilization of the emitter. In addition, we generate coherent states using a microwave source and shot noise with 200 MHz bandwidth using an arbitrary function generator (AFG) at room temperature.

We measure the photon number variance of propagating fields with the qubit setup depicted in Fig. 2(a). To this end, we operate a frequency-tunable transmon qubit at its maximum transition frequency $\omega_q/2\pi = 6.92$ GHz (see Ref. 22 for experimental details). The qubit is coupled with strength $g/2\pi \simeq 67$ MHz to a quarter-wavelength coplanar waveguide resonator with resonance frequency $\omega_r/2\pi = 6.07$ GHz and external coupling rate $\kappa_x/2\pi = 8.5$ MHz. Hence, the system is in the dispersive regime, where the detuning $\delta \equiv \omega_q - \omega_r$ fulfills $\chi \ll g$. Here, [39] $\chi \equiv [g^2/\delta][\alpha/(\delta + \alpha)] \simeq -2\pi \times 3.11$ MHz and $\alpha/2\pi \simeq -315$ MHz is the transmon anharmonicity. In the dispersive regime, the qubit couples to the photon number n_r in the resonator via the interaction Hamiltonian $\mathcal{H}_{\text{int}} = \hbar\chi[n_r + 1/2]\hat{\sigma}_z$. Because the coupling is mediated by the Pauli operator $\hat{\sigma}_z$, temporal fluctuations $n_r(\tau)$ introduce qubit dephasing [43]. More precisely, the fluctuations are characterized by the correlator $\mathcal{C}(\tau) = \langle n_r(0)n_r(\tau) \rangle$ and generate a shift $\delta\varphi(\tau)$ of the qubit phase. While the first moment of this phase shift has a vanishing arithmetic mean, the second moment [44] $\langle \delta\varphi^2 \rangle = 4\chi^2 \int_0^\tau d\tau' \mathcal{C}(\tau')$ enters into the Ramsey decay envelope $\exp[-\gamma_1(n_r)\tau/2 - \langle \delta\varphi^2 \rangle/2]$. Here, $\gamma_1(n_r)$ is the total qubit relaxation rate and $\gamma_{\varphi 0}$ is the qubit dephasing rate due to all other noise sources except for those described by $\mathcal{C}(\tau)$. Thermal fields exhibit a super-Poissonian correlator [45, 46] $\mathcal{C}^{\text{th}}(\tau) = (n_r^2 + n_r) \exp(-\kappa_x\tau)$. The Poissonian nature of coherent states and shot noise inside a resonator follows $\mathcal{C}^{\text{coh}}(\tau) = n_r \exp(-\kappa_x\tau/2)$ and $\mathcal{C}^{\text{sh}}(\tau) = n_r \exp(-\kappa_x\tau)$, respectively. For all three states one obtains $\langle \delta\varphi^2 \rangle/2 = \gamma_{\varphi n}(n_r)\tau$, i.e., an exponential de-

cay envelope. The photon-number-dependent dephasing rates are then defined by [35, 41, 44–46]

$$\gamma_{\varphi n}^{\text{th}}(n_r) = \kappa_x \theta_0^2 (n_r^2 + n_r) \equiv s_0^{\text{th}} (n_r^2 + n_r), \quad (1)$$

$$\gamma_{\varphi n}^{\text{coh}}(n_r) = 2\kappa_x \theta_0^2 n_r \equiv s_0^{\text{coh}} n_r, \quad (2)$$

$$\gamma_{\varphi n}^{\text{sh}}(n_r) = \kappa_x \theta_0^2 n_r \equiv s_0^{\text{sh}} n_r. \quad (3)$$

Here, [44] $\theta_0 = \tan^{-1}(2\chi/\kappa_x)$ is the accumulated phase of the resonator photons due to the interaction with the qubit. Remarkably, the factor two between $\gamma_{\varphi n}^{\text{coh}}$ and $\gamma_{\varphi n}^{\text{sh}}$ is due to the fact that the impact of the fluctuations onto the qubit is larger if the resonator decays slower [43, 45]. For thermal states, we control n_r via the temperature of the emitter, $n_r \propto n(T)$. For coherent states and shot noise, we vary the output power P of the microwave generator, $n_r \propto P$. The exact calibra-

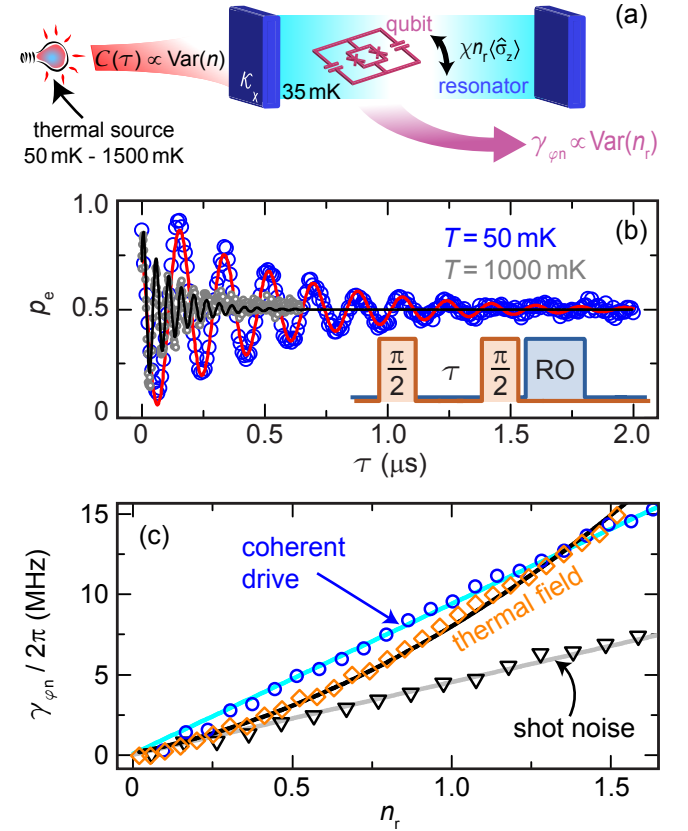


Figure 2. (a) Sketch of the qubit setup. We measure the photon number variance $\text{Var}(n)$ of microwave fields encoded in the photon correlator $\mathcal{C}(\tau)$ by detecting the dephasing rate $\gamma_{\varphi n}$ of a superconducting qubit. (b) Qubit excited state probability p_e for a Ramsey experiment plotted versus waiting time τ between two $\pi/2$ pulses. The solid lines are exponentially decaying sinusoidal fits. The inset shows the Ramsey pulse sequence followed by a readout (RO) pulse. (c) Qubit dephasing rates $\gamma_{\varphi n}$ of prototypical input fields plotted versus the average resonator population n_r . The super-Poissonian $n_r^2 + n_r$ statistics of thermal fields is fitted using Eq. (1). The blue and the grey line are fits of Eq. (2) and Eq. (3) to the data for coherent states and shot noise, respectively.

tion procedure is presented in Ref. 22. As a consequence of Eqs. (1) - (3), measurements of the Ramsey decay rate $\gamma_2(n_r) = \gamma_1(n_r)/2 + \gamma_{\varphi 0} + \gamma_{\varphi n}(n_r)$ allow us to extract the photon number variance as a function of n_r . We obtain $\gamma_1(n_r)$ from an independent measurement [22]. Furthermore, we emphasize that during our sweeps of the attenuator temperature, the sample box is stabilized at 35 mK. Also, all low-frequency components of the thermal field, usually responsible for dephasing, are strongly suppressed by the filter function of the resonator. Therefore, $\gamma_{\varphi 0}$ can be taken as a constant and we can extract $\gamma_{\varphi n}$ from a numerical fit to the decay envelope of a Ramsey time trace.

In the absence of external microwave fields, the transmon qubit is relaxation-limited with the rates $\gamma_1(n_r \approx 0)/2\pi \approx 4$ MHz and $\gamma_2(n_r \approx 0)/2\pi \approx 2$ MHz. In Fig. 2(b), we show the Ramsey time traces for the attenuator temperatures $T = 50$ mK and $T = 1$ K. As expected, the latter shows a significantly increased Ramsey decay rate. A systematic temperature sweep reveals $\gamma_{\varphi n}^{\text{th}}(n_r) \propto n_r^2 + n_r$ as displayed in Fig. 2(c). For small photon numbers $n_r \lesssim 0.5$, we observe that the dephasing rate approaches a linear trend with slope $s_0^{\text{th}} \equiv \partial \gamma_{\varphi n}^{\text{th}} / \partial n_r |_{n_r=0}$. This finite slope clearly allows us to rule out the validity of the classical limit $\text{Var}(n_r) = n_r^2$ in this regime. From a fit of Eq. (1) to the data, we find $s_0^{\text{th}}/2\pi = 3.9$ MHz, which is marginally enhanced compared to the expected value $\kappa_x \theta_0^2/2\pi = 3.4$ MHz. We attribute this slight deviation to a constant thermal background field emitted from attenuators at higher temperature stages and from the sample environment. Applying a beam splitter model [47], we extract the reasonable contribution of $n_c^{\text{th}} = 0.15$ photons. This value corresponds to an effective mode temperature of approximately 140 mK.

As a cross-check for our setup, we confirm the well-explored [20, 35, 44] linear variance of fields with Poissonian photon statistics. To this end, we first expose the resonator to shot noise emitted at room temperature by the AFG [48]. As shown in Fig. 2(c), we indeed find a constant slope $s^{\text{sh}} \equiv \partial \gamma_{\varphi n}^{\text{sh}} / \partial n_r \approx 2\pi \times 4.6$ MHz, which is in reasonable agreement with s_0^{th} . In terms of additional thermal population and effective mode temperature [47], we obtain $n_c^{\text{sh}} \approx 0.19 \approx n_c^{\text{th}}$ and 150 mK, respectively. In the next step, we investigate measurement-induced dephasing caused by coherent states as displayed in Fig. 2(c). We again find a linear slope $s^{\text{coh}} \equiv \partial \gamma_{\varphi n}^{\text{coh}} / \partial n_r \approx 2\pi \times 9.3$ MHz $\approx 2s^{\text{sh}}$. The excellent quantitative agreement with the shot noise result is also reflected in $n_c^{\text{coh}} = n_c^{\text{sh}}$. Due to the enhancement of s^{coh} by a factor of two, the qubit can discriminate between a coherent field and thermal field as well as shot noise already for $n_r \gtrsim 0.3$.

In order to complement our studies of thermal microwaves with the qubit setup, we directly probe field correlations with the dual-path state reconstruction

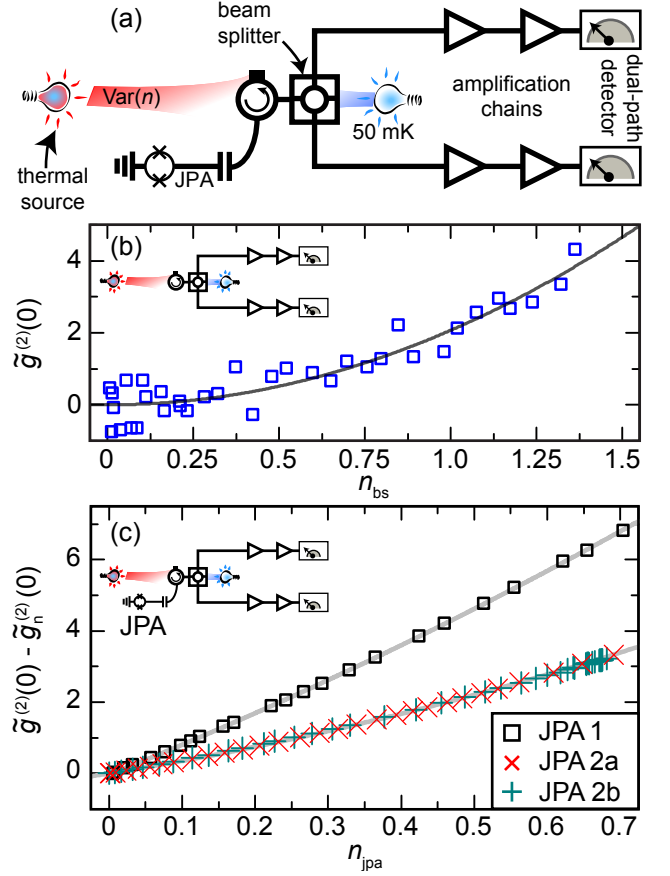


Figure 3. (a) Sketch of the dual-path setup, which we use to directly probe field correlations between two amplification chains behind a cryogenic microwave beam splitter. We can switch on and off the JPA. (b) Unnormalized second-order correlation function $\tilde{g}^{(2)}(0)$ plotted versus photon number n_{bs} at the beam splitter input without using the JPA. The solid line is a fit to the data using the function $\tilde{g}^{(2)}(0) = \rho n_{bs}^2$. (c) Unnormalized second-order correlation function $\tilde{g}^{(2)}(0)$ corrected for the constant offset $\tilde{g}_n^{(2)}(0)$ and plotted versus the photon number n_{jpa} at the JPA input. For the measurements of JPA 2a and JPA 2b we use slightly different operating points described in detail in Ref. 47.

method [12–14, 49]. We use the setup depicted in Fig. 3(a), where a cryogenic beam splitter equally divides the signal along two paths, which are subsequently amplified independently. From the averaged auto- and cross-correlations, we retrieve all signal moments $\langle (\hat{a}^\dagger)^n \hat{a}^m \rangle$ up to fourth order ($0 \leq n + m \leq 4$ with $n, m \in \mathbb{N}_0$) in terms of the annihilation and creation operators, \hat{a} and \hat{a}^\dagger . To calibrate the average photon number $n_{bs} = \langle \hat{a}^\dagger \hat{a} \rangle \propto n(T)$ at the input of the beam splitter, we perform a Planck spectroscopy experiment [12]. More details on the setup can be found in Ref. 15. Notwithstanding the very different experimental requirements in the microwave regime, direct correlation measurements on propagating light fields are inspired from quantum optics. For this reason, we characterize the photon number variance of the thermal

microwave fields via the unnormalized correlation function

$$\tilde{g}^{(2)}(0) \equiv n_{\text{bs}}^2 g^{(2)}(0) = \text{Var}(n_{\text{bs}}) - n_{\text{bs}} + n_{\text{bs}}^2. \quad (4)$$

As shown in Fig. 3(b), the correlation function $\tilde{g}^{(2)}(0)$ of the thermal source follows the expected quadratic behavior. A numerical fit of the polynomial function $\tilde{g}^{(2)}(0) = \rho n_{\text{bs}}^2$ using ρ as a free parameter yields $\rho = 2.07$. This result coincides nicely with $\tilde{g}^{(2)}(0) = 2n_{\text{bs}}^2$ predicted for thermal states by Eq. (4). In the same way as with the qubit setup, we are therefore able to reliably map out the $n^2 + n$ dependence and not only the classical n^2 limit experimentally found in earlier work [11].

To lower the statistical scatter of the data points in Fig. 3(b), we repeat the correlation measurement using a JPA operated in the phase insensitive mode. In this mode, the JPA works as a near-quantum-limited, phase-preserving amplifier [17] with power gain $G \gg 1$. At the input of the beam splitter, one then obtains $n_{\text{bs}} \approx G(n_{\text{jpa}} + n_{\text{n}} + 1)$. Here, $n_{\text{jpa}} \propto n(T)$ are the signal photons and n_{n} are the noise photons added by the JPA, which we again obtain from a Planck spectroscopy experiment [12]. We compare measurements using two different JPAs (JPA 1 and JPA 2) based on frequency-tunable quarter wavelength resonators with operating frequencies $\omega_{\text{jpa}}/2\pi \simeq 5.35$ GHz and typical gains $G \simeq 14$ dB (specific parameters are summarized in Ref. 47). After calibrating for G , we record the modified correlation function

$$\tilde{g}^{(2)}(0) = 2(n_{\text{jpa}} + n_{\text{n}} + 1)^2, \quad (5)$$

which can be derived from an input-output model for the JPA [47]. In Eq. (5), there is an n_{jpa} -independent offset $\tilde{g}_{\text{n}}^{(2)}(0) = 2n_{\text{n}}^2 + 4n_{\text{n}} + 2$ due to the JPA gain and noise. In our model, we assume that the JPA noise is thermal, i.e., $\text{Var}(n_{\text{n}}) = n_{\text{n}}^2 + n_{\text{n}}$.

In Fig. 3(c) we plot the experimentally obtained correlations $\tilde{g}^{(2)}(0) - \tilde{g}_{\text{n}}^{(2)}(0)$ versus the photon number n_{jpa} at the JPA input. From fits to the formula $\rho n_{\text{jpa}}^2 + \xi n_{\text{jpa}}$, we find $\rho \simeq 2.2$ in all three data sets in agreement with the expected value of $\rho = 2$. Therefore, also the JPA assisted measurements confirm a super-Poissonian statistics of the thermal fields. From the fits, we also find that the values ξ is reduced by a factor of approximately 2 compared to the expected value $4 + 4n_{\text{n}}$. This observation is confirmed by the values extracted for $\tilde{g}_{\text{n}}^{(2)}(0)$, which deviate to a similar extent. The reduced experimental values suggest that the JPA noise appears to contain a significant contribution with non-thermal statistics.

Finally, we compare the performance of the qubit and the dual-path setup. Although we operate on and below the single photon level, the qubit and the dual-path setup (without JPA) systematically reproduce the $n^2 + n$ law with a high accuracy. Currently, the statistical spread for the qubit setup is one order of magnitude lower than the one for the dual-path setup. The accuracy of the qubit

setup is limited by the low-frequency variations of the qubit relaxation rate described in Ref. 22. Their standard deviation of 5 % well explains the spread of the experimental data points in Fig. 2(c). Assuming that these variations decrease proportionally to the qubit decoherence rate, we estimate that for the best performing superconducting qubits [41], the accuracy can be improved by at least two orders of magnitude. The dual-path setup (without the JPA) is limited by the data processing rate of our digitizer card and by the noise temperature $T_{\text{n}} \simeq 3$ K of the cryogenic amplifiers. When the JPA is on, the noise temperature of these amplifiers is insignificant. Concerning adaptability, the dual-path setup in principle gives access to all signal moments, whereas the qubit is limited to amplitude and power correlations. While our measurements including a JPA decrease the statistical spread by two orders of magnitude, they also indicate that the statistics of the JPA noise can influence the statistics of the amplified field.

In conclusion, we have quantitatively characterized the photon number variance of propagating thermal microwaves using two fundamentally different approaches: indirect measurements with a superconducting qubit-resonator system and direct ones, with a dual-path detector. With both setups, we are able to quantitatively recover the $n^2 + n$ photon number variance of thermal fields in the single photon regime with a high resolution in comparison with existing experimental achievements [11]. In particular, we analyze the resolution limits and find that they can be improved by several orders of magnitude in both setups. For our current dual-path setup, we make the remarkable observation that noise added by the JPAs has a significant non-thermal contribution. Our results demonstrate that the three types of propagating microwave states we investigate can be reliably distinguished below the single photon level in an experiment by their photon statistics. Therefore, both setups are promising candidates to explore decoherence mechanisms possibly limiting high-performance superconducting qubits [41, 42] and the properties of more advanced quantum microwave states.

The JPAs used in this work are kindly provided by K. Inomata (RIKEN Center for Emergent Matter Science), T. Yamamoto (NEC IoT Device Research Laboratories), and Y. Nakamura (RIKEN, RCAST at the University of Tokyo). We thank E. Solano, R. Di Candia, M. Sanz (Department of Physical Chemistry, University of the Basque Country) for fruitful discussions on the correlation measurement setup. We acknowledge financial support from the German Research Foundation through SFB 631 and FE 1564/1-1, EU projects CCQED, PROMISCE, the doctorate programs ExQM of the Elite Network of Bavaria, and the International Max Planck Research School "Quantum Science and Technology".

* jan.goetz@wmi.badw.de

† rudolf.gross@wmi.badw.de

- [1] D. Bouwmeester, J.-W. Pan, K. Mattle, M. Eibl, H. Weinfurter, and A. Zeilinger, *Nature* **390**, 575 (1997).
- [2] A. Furusawa, J. L. Sørensen, S. L. Braunstein, C. A. Fuchs, H. J. Kimble, and E. S. Polzik, *Science* **282**, 706 (1998).
- [3] P. Kok, W. J. Munro, K. Nemoto, T. C. Ralph, J. P. Dowling, and G. J. Milburn, *Rev. Mod. Phys.* **79**, 135 (2007).
- [4] S. L. Braunstein and P. van Loock, *Rev. Mod. Phys.* **77**, 513 (2005).
- [5] U. L. Andersen, J. S. Neergaard-Nielsen, P. van Loock, and A. Furusawa, *Nat. Phys.* **11**, 713 (2015).
- [6] R. Di Candia, K. G. Fedorov, L. Zhong, S. Felicetti, E. P. Menzel, M. Sanz, F. Deppe, A. Marx, R. Gross, and E. Solano, *EPJ Quant. Tech.* **2**, 25 (2015).
- [7] S. Lloyd, *Science* **321**, 1463 (2008).
- [8] S.-H. Tan, B. I. Erkmen, V. Giovannetti, S. Guha, S. Lloyd, L. Maccone, S. Pirandola, and J. H. Shapiro, *Phys. Rev. Lett.* **101**, 253601 (2008).
- [9] E. D. Lopaeva, I. Ruo Berchera, I. P. Degiovanni, S. Olivares, G. Brida, and M. Genovese, *Phys. Rev. Lett.* **110**, 153603 (2013).
- [10] S. Barzanjeh, S. Guha, C. Weedbrook, D. Vitali, J. H. Shapiro, and S. Pirandola, *Phys. Rev. Lett.* **114**, 080503 (2015).
- [11] J. Gabelli, L.-H. Reydellet, G. Fève, J.-M. Berroir, B. Plaças, P. Roche, and D. C. Glattli, *Phys. Rev. Lett.* **93**, 056801 (2004).
- [12] M. Mariani, E. P. Menzel, F. Deppe, M. A. Araque Caballero, A. Baust, T. Niemczyk, E. Hoffmann, E. Solano, A. Marx, and R. Gross, *Phys. Rev. Lett.* **105**, 133601 (2010).
- [13] E. P. Menzel, F. Deppe, M. Mariani, M. A. Araque Caballero, A. Baust, T. Niemczyk, E. Hoffmann, A. Marx, E. Solano, and R. Gross, *Phys. Rev. Lett.* **105**, 100401 (2010).
- [14] E. P. Menzel, R. Di Candia, F. Deppe, P. Eder, L. Zhong, M. Ihmig, M. Haeberlein, A. Baust, E. Hoffmann, D. Ballester, K. Inomata, T. Yamamoto, Y. Nakamura, E. Solano, A. Marx, and R. Gross, *Phys. Rev. Lett.* **109**, 250502 (2012).
- [15] K. G. Fedorov, L. Zhong, S. Pogorzalek, P. Eder, M. Fischer, J. Goetz, E. Xie, F. Wulschner, K. Inomata, T. Yamamoto, Y. Nakamura, R. Di Candia, U. Las Heras, M. Sanz, E. Solano, E. P. Menzel, F. Deppe, A. Marx, and R. Gross, *Phys. Rev. Lett.* **117**, 020502 (2016).
- [16] F. Mallet, M. A. Castellanos-Beltran, H. S. Ku, S. Glancy, E. Knill, K. D. Irwin, G. C. Hilton, L. R. Vale, and K. W. Lehnert, *Phys. Rev. Lett.* **106**, 220502 (2011).
- [17] L. Zhong, E. P. Menzel, R. Di Candia, P. Eder, M. Ihmig, A. Baust, M. Haeberlein, E. Hoffmann, K. Inomata, T. Yamamoto, Y. Nakamura, E. Solano, F. Deppe, A. Marx, and R. Gross, *New J. Phys.* **15**, 125013 (2013).
- [18] C. Macklin, K. O'Brien, D. Hover, M. E. Schwartz, V. Bolkhovskiy, X. Zhang, W. D. Oliver, and I. Siddiqi, *Science* **350**, 307 (2015).
- [19] C. Eichler, D. Bozyigit, C. Lang, L. Steffen, J. Fink, and A. Wallraff, *Phys. Rev. Lett.* **106**, 220503 (2011).
- [20] A. P. Sears, A. Petrenko, G. Catelani, L. Sun, H. Paik, G. Kirchmair, L. Frunzio, L. I. Glazman, S. M. Girvin, and R. J. Schoelkopf, *Phys. Rev. B* **86**, 180504 (2012).
- [21] K. W. Murch, S. J. Weber, K. M. Beck, E. Ginossar, and I. Siddiqi, *Nature* **499**, 62 (2013).
- [22] J. Goetz, F. Deppe, P. Eder, M. Fischer, M. Müting, J. P. Martínez, S. Pogorzalek, F. Wulschner, E. Xie, K. G. Fedorov, A. Marx, and R. Gross, ArXiv e-prints (2016), [arXiv:1609.07351](https://arxiv.org/abs/1609.07351) [quant-ph].
- [23] D. M. Meekhof, C. Monroe, B. E. King, W. M. Itano, and D. J. Wineland, *Phys. Rev. Lett.* **76**, 1796 (1996).
- [24] M. Brune, F. Schmidt-Kaler, A. Maali, J. Dreyer, E. Hagley, J. M. Raimond, and S. Haroche, *Phys. Rev. Lett.* **76**, 1800 (1996).
- [25] M. Hofheinz, E. M. Weig, M. Ansmann, R. C. Bialczak, E. Lucero, M. Neeley, A. D. O'Connell, H. Wang, J. M. Martinis, and A. N. Cleland, *Nature* **454**, 310 (2008).
- [26] D. I. Schuster, A. A. Houck, J. A. Schreier, A. Wallraff, J. M. Gambetta, A. Blais, L. Frunzio, J. Majer, B. Johnson, M. H. Devoret, S. M. Girvin, and R. J. Schoelkopf, *Nature* **445**, 515 (2007).
- [27] B. L. Morgan and L. Mandel, *Phys. Rev. Lett.* **16**, 1012 (1966).
- [28] F. Arecchi, E. Gatti, and A. Sona, *Phys. Lett.* **20**, 27 (1966).
- [29] P. K. Tan, G. H. Yeo, H. S. Poh, A. H. Chan, and C. Kurtsiefer, *Astrophys. J. Lett.* **789**, L10 (2014).
- [30] R. Short and L. Mandel, *Phys. Rev. Lett.* **51**, 384 (1983).
- [31] G. Rempe, F. Schmidt-Kaler, and H. Walther, *Phys. Rev. Lett.* **64**, 2783 (1990).
- [32] F. Treussart, R. Alléaume, V. Le Floch, L. T. Xiao, J.-M. Courty, and J.-F. Roch, *Phys. Rev. Lett.* **89**, 093601 (2002).
- [33] R. Hanbury Brown and R. Q. Twiss, *Nature* **177**, 27 (1956).
- [34] R. Hanbury Brown and R. Q. Twiss, *Nature* **178**, 1046 (1956).
- [35] D. I. Schuster, A. Wallraff, A. Blais, L. Frunzio, R.-S. Huang, J. Majer, S. M. Girvin, and R. J. Schoelkopf, *Phys. Rev. Lett.* **94**, 123602 (2005).
- [36] A. A. Houck, D. I. Schuster, J. M. Gambetta, J. A. Schreier, B. R. Johnson, J. M. Chow, L. Frunzio, J. Majer, M. H. Devoret, S. M. Girvin, and R. J. Schoelkopf, *Nature* **449**, 328 (2007).
- [37] J.-C. Forgues, C. Lupien, and B. Reulet, *Phys. Rev. Lett.* **113**, 043602 (2014).
- [38] Y. Blanter and M. Büttiker, *Phys. Rep.* **336**, 1 (2000).
- [39] J. Koch, T. M. Yu, J. Gambetta, A. A. Houck, D. I. Schuster, J. Majer, A. Blais, M. H. Devoret, S. M. Girvin, and R. J. Schoelkopf, *Phys. Rev. A* **76**, 042319 (2007).
- [40] T. Yamamoto, K. Inomata, M. Watanabe, K. Matsuba, T. Miyazaki, W. D. Oliver, Y. Nakamura, and J. S. Tsai, *Appl. Phys. Lett.* **93**, 042510 (2008).
- [41] C. Rigetti, J. M. Gambetta, S. Poletto, B. L. T. Plourde, J. M. Chow, A. D. Córcoles, J. A. Smolin, S. T. Merkel, J. R. Rozen, G. A. Keefe, M. B. Rothwell, M. B. Ketchen, and M. Steffen, *Phys. Rev. B* **86**, 100506 (2012).
- [42] F. Yan, S. Gustavsson, A. Kamal, J. Birenbaum, A. P. Sears, D. Hover, D. Rosenberg, G. Samach, T. J. Gudmundsen, J. L. Yoder, T. P. Orlando, J. Clarke, A. J. Kerman, and W. D. Oliver, ArXiv e-prints (2015), [arXiv:1508.06299](https://arxiv.org/abs/1508.06299).
- [43] A. Blais, R.-S. Huang, A. Wallraff, S. M. Girvin, and R. J. Schoelkopf, *Phys. Rev. A* **69**, 062320 (2004).

- [44] J. Gambetta, A. Blais, D. I. Schuster, A. Wallraff, L. Frunzio, J. Majer, M. H. Devoret, S. M. Girvin, and R. J. Schoelkopf, *Phys. Rev. A* **74**, 042318 (2006).
- [45] P. Bertet, I. Chiorescu, C. Harmans, and J. Mooij, *ArXiv e-prints* (2005), [arXiv:cond-mat/0507290 \[cond-mat\]](#).
- [46] P. Bertet, I. Chiorescu, G. Burkard, K. Semba, C. J. P. M. Harmans, D. P. DiVincenzo, and J. E. Mooij, *Phys. Rev. Lett.* **95**, 257002 (2005).
- [47] See Supplemental Material for experimental techniques and theoretical methods.
- [48] J. M. Fink, L. Steffen, P. Studer, L. S. Bishop, M. Baur, R. Bianchetti, D. Bozyigit, C. Lang, S. Filipp, P. J. Leek, and A. Wallraff, *Phys. Rev. Lett.* **105**, 163601 (2010).
- [49] R. Di Candia, E. P. Menzel, L. Zhong, F. Deppe, A. Marx, R. Gross, and E. Solano, *New J. Phys.* **16**, 015001 (2014).
- [50] C. M. Caves, *Phys. Rev. D* **26**, 1817 (1982).

Supplemental Materials: Photon Statistics of Propagating Thermal Microwaves

SAMPLE DETAILS AND EXPERIMENTAL SETUP

For the measurements based on the qubit setup, we use the experimental setup presented in Ref. 22. For the measurements based on the dual-path setup, we use the experimental setup presented in Ref. 15. This setup comprises a flux-driven Josephson parametric amplifier (JPA) with gain G consisting of a quarter-wavelength transmission line resonator, which is short-circuited to the ground by a DC SQUID. We couple an on-chip antenna inductively to the DC SQUID loop to apply a strong coherent pump tone ω_p at approximately twice the resonant frequency ω_{jpa} of the JPA. This pump scheme amplifies the incoming signal with a typical gain G as summarized in Tab. I.

PHOTON NUMBER VARIANCE OF ATTENUATED AND AMPLIFIED SIGNALS

In this section, we discuss how attenuation (loss) and amplification processes modify the photon statistics of a signal. We describe the attenuation process with a beam splitter model. The attenuation factor η translates into the splitting ratio of the device and a thermal state with population n_c is incident of the second input port. We define the thermal state emitted by the heatable attenuator with the bosonic operators \hat{b}^\dagger and \hat{b} and $n = \langle \hat{b}^\dagger \hat{b} \rangle$. Similarly, the background thermal photons are defined by \hat{c}^\dagger and \hat{c} leading to $n_c = \langle \hat{c}^\dagger \hat{c} \rangle$. That way, we obtain $\hat{a}(t) = \sqrt{\eta} \hat{b}(t) + \sqrt{1-\eta} \hat{c}(t)$ for the attenuated input state leading to the total photon number $n_t = \langle \hat{a}^\dagger \hat{a} \rangle = \eta n + (1-\eta)n_c$. Then, following Ref. 43, the correlator

$$\begin{aligned} \mathcal{C}^{\text{th}}(\tau) &= \langle (\hat{a}^\dagger \hat{a} - \langle \hat{a}^\dagger \hat{a} \rangle)^2 \rangle \exp(-\kappa_x \tau) \\ &= [\eta^2 n^2 + \eta n + 2\eta(1-\eta)nn_c + (1-\eta)^2 n_c^2 + (1-\eta)n_c] \exp(-\kappa_x \tau) \end{aligned} \quad (\text{S1})$$

describes the total field entering the resonator. From Eq. (S1) we see that the beam splitter model predicts the thermal photon statistics of the emitted field for $\eta \mapsto 1$ (no background field) and the thermal photon statistics of the background field for $\eta \mapsto 0$ (strong background field). In a similar way, we calculate the correlator of an attenuated coherent field

$$\begin{aligned} \mathcal{C}^{\text{coh}}(\tau) &= \langle (\hat{a}^\dagger \hat{a} - \langle \hat{a}^\dagger \hat{a} \rangle)^2 \rangle \exp(-\kappa_x \tau / 2) \\ &= [\eta n + 2\eta(1-\eta)nn_c + (1-\eta)^2 n_c^2 + (1-\eta)n_c] \exp(-\kappa_x \tau / 2), \end{aligned} \quad (\text{S2})$$

which approaches the variance of a coherent state for $\eta \mapsto 1$ and the thermal photon statistics of the cold attenuator for $\eta \mapsto 0$.

Table I. Overview of the JPA samples. We perform one measurement with JPA 1 and two individual measurements using JPA 2 with different detunings $\delta_{jpa} = \omega_{jpa} - \omega_p/2$ between JPA frequency ω_{jpa} and pump frequency ω_p . The measurement bandwidth for all measurements is $\omega_{jpa} \pm 200$ kHz.

device	run	gain G	n_n	ρ	ξ	$\tilde{g}_n^{(2)}(0)$	$\delta_{jpa}/2\pi$	$\omega_{jpa}/2\pi$
JPA 1	-	14.5 dB	1.71	2.24	8.14	7.1	100 kHz	5.4 GHz
JPA 2	a	13.9 dB	0.66	2.23	3.29	1.1	100 kHz	5.4 GHz
JPA 2	b	15.2 dB	0.97	2.21	3.29	1.8	500 kHz	5.3 GHz

Similar to the calculations of attenuated propagating microwaves, we calculate the variance of an amplified thermal field using input-output relations. Following Ref. 49 and Ref. 50, we describe the amplified field by the operator $\hat{a}(t) = \sqrt{G}\hat{b} + \sqrt{G-1}\hat{c}^\dagger$, where $n_{\text{bs}} = \langle \hat{a}^\dagger \hat{a} \rangle$. The quantity $n_{\text{n}} = \langle \hat{c}^\dagger \hat{c} \rangle$ describes the noise photons added by the JPA, which we assume to be thermal. Based on these assumptions, we obtain the photon number variance

$$\begin{aligned} \text{Var}(n_{\text{bs}}) &= \langle (\hat{a}^\dagger \hat{a} - \langle \hat{a}^\dagger \hat{a} \rangle)^2 \rangle \\ &= G^2 n_{\text{jpa}}^2 + G^2 n_{\text{jpa}} + G(G-1)n_{\text{jpa}} + 2G(G-1)n_{\text{jpa}}n_{\text{n}} \\ &\quad + (G-1)^2 n_{\text{n}}^2 + (G-1)^2 n_{\text{n}} + G(G-1)n_{\text{n}} + G(G-1), \end{aligned} \quad (\text{S3})$$

which approaches the variance $n_{\text{jpa}}^2 + n_{\text{jpa}}$ of a thermal state for $G \mapsto 1$ (no amplification). For strong amplification ($G \gg 1$), we obtain $\text{Var}(n_{\text{bs}}) \approx G^2(n_{\text{jpa}} + n_{\text{n}} + 1)^2 = n_{\text{bs}}^2$. As a consequence, the unnormalized $g^{(2)}$ function of the amplified field becomes

$$\tilde{g}^{(2)}(0) \equiv n_{\text{bs}}^2 g^{(2)}(0) = \text{Var}(n_{\text{bs}}) - n_{\text{bs}} + n_{\text{bs}}^2 \approx 2G^2(n_{\text{jpa}} + n_{\text{n}} + 1)^2. \quad (\text{S4})$$

We fit this relation to our data as discussed in the main text.